Modeling the properties of MgAgSb, a promising thermoelectric material for use in the temperature range of 300–600 K

© V.G. Orlov, G.S. Sergeev, A.A. Ivanov

National Research Center „Kurchatov Institute“,
123182 Moscow, Russia

E-mail: valeryorlov3@gmail.com

Received September 24, 2025
Revised October 10, 2025
Accepted November 5, 2025

Using the WIEN2k program, based on the density functional method, the electronic structure of the tetragonal α- and β-phases and two variants of the cubic γ-phases of the MgAgSb compound was calculated. From the calculation results it follows that the structural phase transitions in MgAgSb are accompanied by semiconductor-metal electronic transitions. Analysis of the features in the spatial distribution of the charge density of the α- and β- and γ-phases showed the absence of covalent bonding in MgAgSb, which can explain the presence of several structural phase transitions over a small temperature range. Using the phonopy and phono3py programs, the phonon spectra of the γ-phase of MgAgSb, as well as its lattice thermal conductivity in the temperature range from 300 to 1000 K, were calculated. The IRelast program made it possible to find for all MgAgSb phases both the values of the elastic constants C_{ij} and the values of the main strength characteristics — shear moduli, compression moduli, Young's modulus, Poisson's ratio, Vickers hardness, and universal indices of elastic property anisotropy. Basing on the analysis of the obtained data, it was concluded that the α-phase of MgAgSb has the best mechanical properties.

Keywords: thermoelectric material, electronic structure calculations, phonon spectra, lattice thermal conductivity, strength mechanical properties.

DOI: 10.61011/SC.2025.07.62474.8590

1. Introduction

The compound α-MgAgSb is considered as a promising thermoelectric material (TEM), which demonstrates the possibility of creating thermoelectric generators with an efficiency of up to 12% in the temperature range from 300 to 600 K [1–3]. High conversion efficiency is provided by large values [1–5] of dimensionless thermoelectric Q-factor ZT:

$$ZT = \frac{S^2\sigma}{\kappa_{\text{lat}} + \kappa_{\text{el}}} T, \qquad (1)$$

where T is the temperature, S is the thermo-emf (Seebeck coefficient), σ is the electrical conductivity, κ_{lat} is the thermal conductivity of the lattice and κ_{el} is the thermal conductivity of charge carriers (electrons and holes). It should be noted that the maximum value of $ZT \sim 1.6$ at $T = 523$ K was obtained in Ref. [1] for α-MgAgSb samples, the composition of which was close to stoichiometric.

The presence of two more phases such as tetragonal β and cubic γ was revealed in MgAgSb compound in Ref. [6] using X-ray diffraction, in addition to the low-temperature tetragonal α-phase. The temperature range in which the new phases exist has turned out to be quite narrow: β-phase was found at a temperature of 300 °C and γ-phase was found at a temperature of 360 °C. The presence of three crystalline phases in MgAgSb was confirmed in Ref. [7]. But the variant of the arrangement of atoms in the lattice cell proposed for the γ-phase differs from the arrangement of atoms proposed in Ref. [6]. Further, we will denote the γ-phases of MgAgSb with the arrangement of atoms from Refs. [6 and 7] as $\gamma 1$ and $\gamma 2$, respectively.

Taking into account the reported [4,7–11] spread of the results of calculations of the electronic structure of various phases of the MgAgSb compound, as well as the importance of the question of the type of chemical bonding realized in this compound, it seemed interesting to use for calculations of the electronic structure and analysis of features in the charge distribution of α-, β-, $\gamma 1$- and $\gamma 2$-phases of MgAgSb, the approach that was previously used to model the properties of phase change materials [12,13], antimony and bismuth chalcogenides [14,15], high-temperature superconductors and the parent compounds for obtaining them [16–18]. This approach for calculation of the electronic band structure consists of using a software package WIEN2k [19,20], exchange potential mBJ [21] and electronic correlations in a local charge density approximation [22]. The singularities in the charge density distribution and their analysis were found using the CRITIC2 [23] program, developed for the topological analysis of scalar fields in periodic lattices based on the method „Quantum Theory of Atoms in Molecules and Crystals“ [24–26].

High values of ZT (1) for α-MgAgSb are associated both with a low value of total thermal conductivity $\kappa_{\text{tot}} = \kappa_{\text{lat}} + \kappa_{\text{el}}$, and mainly with low lattice thermal conductivity κ_{lat}. The experimental values of $\kappa_{\text{tot}} \sim 1\,\text{W}\cdot\text{m}^{-1}\cdot\text{K}^{-1}$ for α-MgAgSb at room temperature are given in Refs. [4–7,27]. The lattice thermal conductivity

Table 1. Parameters of MgAgSb crystal phases

Phase, reference	Space group	Z	Parameters of lattices	Atom	Position type, coordinates of atoms
α [6]	Tetragonal $I\bar{4}c2\ D_{2d}^{10}$ N120	16	$a = b = 9.176$ Å $c = 12.696$ Å	Mg Ag1 Ag2 Ag3 Sb	16i; −0.036, 0.296, 0.096 4a; 0, 0, 1/4 4b; 0, 0, 0 8e; 0.224, 0.224, 1/4 16i; 0.236, 0.475, 0.12
β [6]	Tetragonal $P4/nmm\ D_{4h}^{7}$ N129	2	$a = b = 4.4199$ Å $c = 6.8896$	Mg Ag Sb	2c; 1/4, 1/4, 0.333 2a; 3/4, 1/4, 0 2c; 1/4, 1/4, 0.729
$\gamma 1$ [6]	Cubic $F\bar{4}3m\ T_d^2$ N216	4	$a = b = c = 6.700$ Å	Mg Ag Sb	4b; 1/2, 1/2, 1/2 4c; 1/4, 1/4, 1/4 4a; 0, 0, 0
$\gamma 2$ [7]	Cubic $F\bar{4}3m\ T_d^2$ N216	4	$a = b = c = 6.704$ Å	Mg Ag Sb	4a; 0, 0, 0 4b; 1/2, 1/2, 1/2 4c; 1/4, 1/4, 1/4

κ_{lat} is usually estimated by subtracting from κ_{tot} the contribution to the thermal conductivity of charge carriers κ_{el} calculated according to the Wiedemann-Franz law:

$$\kappa_{el} = L\sigma T, \tag{2}$$

where L is the Lorentz number, σ is the measured electrical conductivity, T is the temperature. In this case, there is a significant uncertainty associated with both the applicability of formula (2) and the Lorentz number (L), which, even at room temperature, may differ markedly from its value for free electrons in a metal, and may depend on the details of the band structure, electron and phonon scattering mechanisms, and temperature [28]. The value κ_{lat} in Refs. [4–7,27] for α-MgAgSb at room temperature, found by subtracting the contribution of κ_{el} (2) from κ_{tot}, was estimated as $\kappa_{lat} \sim 0.6-0.8\ W \cdot m^{-1} \cdot K^{-1}$. The reasons for the low values of κ_{lat} in experimental and theoretical studies in Refs. [4–7,9,27,29–31]: lattice defects, the presence of impurities, the specificity of chemical bonding and the anharmonicity of atomic vibrations. Given the considerable uncertainty of estimation of κ_{lat} using the procedure described above, it seemed interesting to calculate the spectra of atomic vibrations and the lattice thermal conductivity of the MgAgSb compound using the phonopy [32] and phono3py [33] programs. The complexity of the crystal structure of the α-phase of MgAgSb, whose tetragonal lattice cell contains 16 formula units of the compound (48 atoms), requires long computer calculations, therefore, calculations in this paper were performed for $\gamma 1$-phase of MgAgSb.

In addition to the high values of ZT (1), thermoelectric materials must also have good strength properties, since they have to work for a long time under cyclic thermal loads. The mechanical properties of tetragonal α-, β- and cubic $\gamma 1$-, $\gamma 2$-phases of the MgAgSb compound were modeled in this study using the IRelast program [34], implemented in the WIEN2k software package [19].

2. Electronic band structure and charge density distribution features in MgAgSb

Calculations of the electronic band structure of tetragonal α-, β- and cubic $\gamma 1$-, $\gamma 2$-phases of the MgAgSb compound were carried out using the WIEN2k software package [19,20] based on the density functional theory (DFT) method An Augmented Plane Wave + Local Orbitals. The Becke and Johnson exchange potential (mBJ), modified by Tran and Blaha [21], was chosen as the exchange potential, which includes the charge density and its gradient, as well as the kinetic energy density of electrons. The electronic correlations were taken into account in the local density approximation (LDA) [22].

The experimental values of the structural parameters of the MgAgSb crystal phase lattice from Refs. [6,7] and listed in Table 1 were used for calculations. In particular, Table 1 presents: the names of the crystalline phases of the MgAgSb compound, references to structural works, the name and number of the space group describing the crystalline symmetry of the phase, the number of formula units in the lattice cell, lattice parameters, types of positions occupied by atoms, coordinates of one of the positions of this type, expressed as fractions of the lattice parameters. The symbols and numbers of the space groups in Table 1 are given in the designations of the International Tables on Crystallography [35].

According to the recommendations [19,20] the states of Mg, Ag, and Sb electrons with energies lower than −6 rydberg, were considered as core states. Mg 3s-electrons, Ag 4d- and 5s-electrons, Sb 5s- and 5p-electrons were

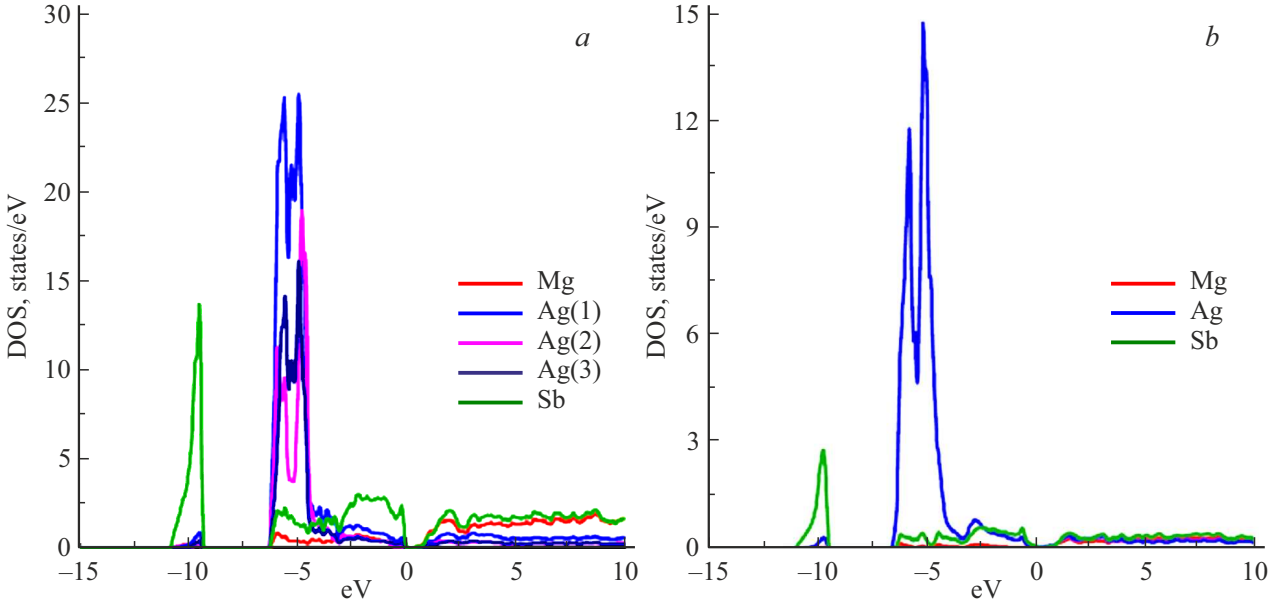

Figure 1. Total densities of energy states for electrons of atoms included in the composition: *a* — α-MgAgSb, *b* — β-MgAgSb.

considered as valence. The calculations were carried out taking into account the spin-orbit interaction of electrons in the atoms that make up the compound. To ensure the necessary accuracy, the following parameters were used in the calculations: decomposition by l-orbital moment was performed inside atomic spheres up to $l_{\max} = 10$, the radii of atomic spheres $R_{\min}$ for Mg, Ag and Sb were taken to be 2.0, 2.2 and 2.3 a.u., respectively. The value of the maximum wave vector $\kappa_{\max}$ used in the plane wave decomposition was determined from the condition $R_{\min} \cdot \kappa_{\max} = 6.5$, and the total number of points in the Brillouin zone was 1000. The convergence criterion for total energy was taken to be 10^{-5} rydberg.

Since the tetragonal lattice cell of α-MgAgSb contains 16 formula units (48 atoms), the picture of the electronic band structure seems to be uninformative. As a result, we present in Figure 1, *a* the total densities of energy states (DOS) of valence electrons and conduction band electrons for the atoms that make up the α-phase of the MgAgSb compound.

The peak in the density of states near -10 eV is mainly attributable to Sb s-electrons. d-electrons of three types of Ag atoms gave a high density of states in the energy range from -6 to -4 eV. The valence band from -4 to 0 eV is represented by Sb p-electrons, as well as s-electrons of Ag and Mg. Calculations revealed the presence of a small energy gap of ~ 0.4 eV in α-MgAgSb. For comparison, Figure 1, *b* shows the total densities of energy states (DOS) of valence electrons and conduction band electrons for the atoms that make up the β-phase of the MgAgSb compound. Unlike the α-phase, the β-phase of MgAgSb turned out to be a metal, but with a very low density of states on the Fermi surface.

For the two variants of the arrangement of atoms in the lattice cell of the γ-phase, the electronic band structure was noticeably different, as can be seen in Figure 2, *a, b*.

The main contribution to the valence band states from -4 to 0 eV is made by Ag d- and s-electrons, Sb p-electrons and Mg s-electrons. As follows from Figure 2, *a, b*, the MgAgSb $\gamma 1$-phase is a metal, while the $\gamma 2$-phase has a noticeable semiconductor gap of ~ 0.8 eV.

The charge density distributions in lattice cells of α-, β- and γ-phases of the MgAgSb compound obtained as a result of calculations using the WIEN2k program were analyzed using the CRITIC2 program [23]. The purpose of the analysis is to find bond critical points (BCPs) in the charge density distribution (the charge density gradient vanishes in them, two eigenvalues of the Hessian matrix of the second derivatives of the charge density over coordinates are negative, and the third eigenvalue is positive) and their parameters to identify the types of chemical bonding in the α-, β- and γ-phases of the MgAgSb compound. The results are presented in Table 2. In particular, Table 2 shows which atoms are bonded, the distance d between the bonded atoms, the number of BCPs of this type for the first atom of a pair of bonded atoms, and the BCPs parameters: the ratio of the moduli of two negative eigenvalues of the Hessian matrix to the third positive eigenvalue $|\lambda_{1,2}|/\lambda_3$, the value of which characterizes the degree of bond covalence, the sign and magnitude of the charge density Laplacian in BCP $\Delta\rho_b$, the value of the charge density ρ_b in BCP, N_{at} is the total number of BCPs for nonequivalent atoms in the lattice cell of the compound, as well as the values of an important dimensionless parameter of the flatness f comprising the ratio of the minimum charge density at a critical point of the cage type $\rho_c^{\min}$ to the maximum charge density in BCPs $\rho_b^{\max}$, which characterizes the uniformity

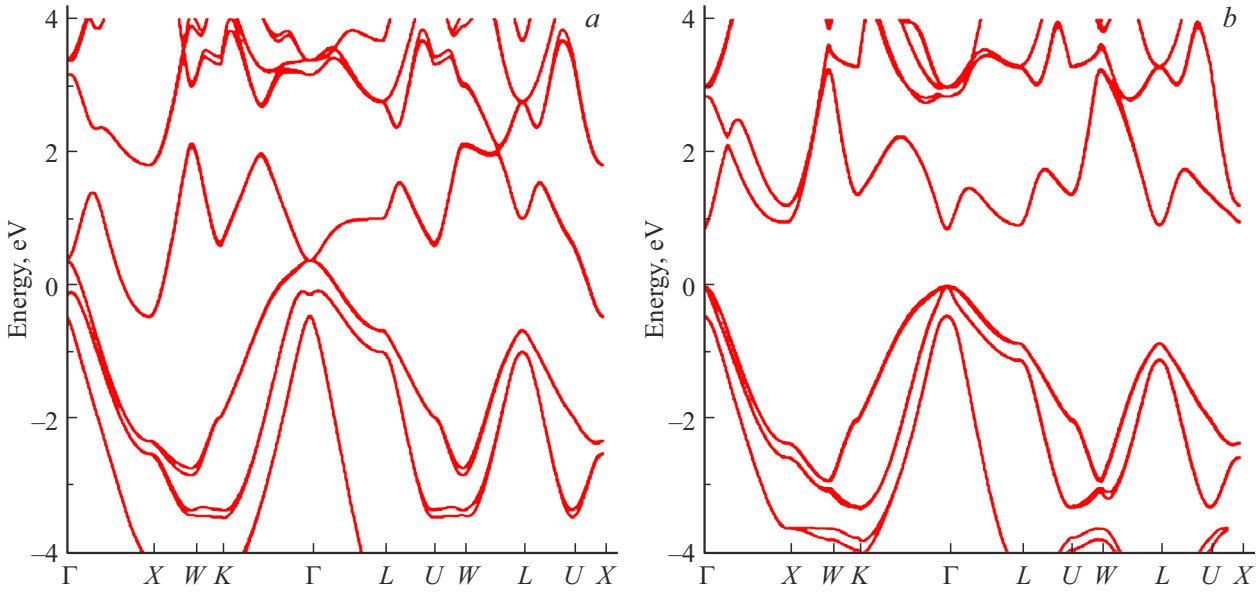

Figure 2. The electronic band structure of γ-phases of the MgAgSb compound, calculated for the arrangement of atoms in the lattice cell of the compound: *a* — $\gamma 1$, *b* — $\gamma 2$.

Table 2. Parameters of bond type critical points for MgAgSb α-, β-, $\gamma 1$- and $\gamma 2$-phases

Phase	N	Bonded atoms	d, Å	N_b	$\lvert\lambda_{1,2}\rvert/\lambda_3$	$\Delta\rho_b$, e/Å^5	ρ_b, e/Å^3	f, %	N_{at}
α-phase	b_1	Ag1−Sb	2.843	2	0.270	0.996	0.294	5.9	$N_{Mg} = 3$
	b_2	Sb−Ag1	2.830	1	0.266	1.038	0.291		$N_{Ag1} = 5$
	b_3	Ag3−Sb	2.871	4	0.246	1.109	0.277		$N_{Ag2} = 8$
	b_4	Sb−Ag2	2.936	1	0.215	1.18	0.243		$N_{Ag3} = 6$
	b_5	Ag2−Ag1	2.912	2	0.143	1.75	0.189		$N_{Sb} = 7$
	b_6	Sb−Mg	2.809	1	0.161	1.75	0.177		
	b_7	Mg−Sb	2.818	1	0.164	1.71	0.177		
	b_8	Mg−Sb	3.006	1	0.152	1.123	0.125		
	b_9	Ag3−Ag2	3.174	2	0.121	1.386	0.123		
β-phase	b_1	Sb−Ag	2.892	4	0.179	1.740	0.255	10	$N_{Mg} = 5$
	b_2	Sb−Mg	2.730	1	0.170	2.075	0.195		$N_{Ag} = 4$
	b_3	Sb−Mg	3.155	4	0.203	0.504	0.100		$N_{Sb} = 9$
$\gamma 1$-phase	b_1	Sb−Ag	2.901	4	0.252	1.021	0.268	4	$N_{Mg} = 4$
	b_2	Ag−Mg	2.901	4	0.109	0.721	0.101		$N_{Ag} = 8$
									$N_{Sb} = 4$
$\gamma 2$-phase	b_1	Ag−Sb	2.901	4	0.224	1.205	0.249	3	$N_{Mg} = 4$
	b_2	Mg−Sb	2.901	4	0.168	1.455	0.153		$N_{Ag} = 4$
									$N_{Sb} = 8$

of the charge density distribution in the crystal. For alkali metals, the values of f are close to 100 % [24–26].

It follows from Table 2 that all MgAgSb phases lack a covalent bonding type, characterized by negative values of the charge density Laplacian $\Delta\rho_b$ in BCPs, which indicate charge leakage in the region near BCPs, values of the ratio $|\lambda_{1,2}|/\lambda_3$ exceeding unity, as well as large values of charge density ρ_b in BCPs [24–26]. The type of chemical bonding in all MgAgSb phases turned out to be similar to the type of bonding previously identified in phase change materials based on $(GeTe)_m-(Sb_2Te_3)_n$ alloys [12,13], which are supposed to be used for the manufacture of non-volatile electronic memory (they are also effective thermoelectrics), as well as in high-temperature superconductors and parent compounds for their obtaining [16–18]. This type of chemical bonding is characterized by positive values of charge density Laplacian $\Delta\rho_b$ in BCPs, indicating the ejection of charge density from regions near BCPs, noticeable values

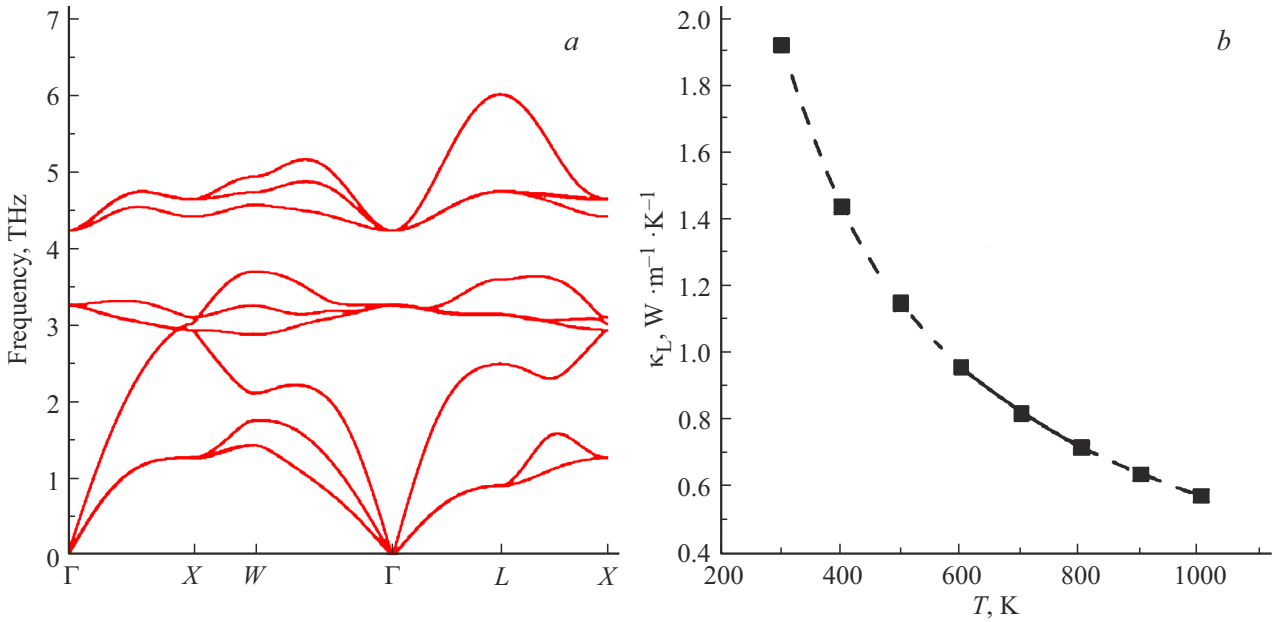

Figure 3. Spectra of atomic vibrations in the lattice of MgAgSb $\gamma 1$-phase (a), temperature dependence of lattice thermal conductivity of MgAgSb $\gamma 1$-phase (b).

of charge density ρ_b in BCPs, large total numbers of N_{at} BCPs, significantly exceeding the valence of atoms, as well as small values of the parameter f. This type of chemical bonding can cause fluctuations of charge density in a sample, similar to those recently detected by the resonant inelastic X-ray scattering (RIXS) method in almost all high-temperature superconductors containing copper [36,37]. It may be the reason for the existence of several structural phase transitions in the MgAgSb compound over a small temperature range, as well as low values of lattice thermal conductivity.

3. Calculations of vibrational spectra and lattice thermal conductivity of MgAgSb γ-phase

Due to the complexity of the crystal structure of the α-phase, calculations of its vibrational spectra and lattice thermal conductivity require long computer operating times, so it was decided to limit the calculation to modeling the lattice properties of the MgAgSb γ-phase using computer programs phonopy [32] and phono3py [33]. In addition, the $\gamma 1$ variant of the arrangement of atoms in the lattice cell was chosen, since the $\gamma 2$ variant gives negative frequency values for a number of branches of atomic vibrations [7]. The method of supercells with a finite displacement of atoms (finite-displacement supercell approach) was used for calculations. A set of supercells with dimension $2\times2\times2$ with finite atomic displacements was generated based on data on the parameters of the crystal structure of the MgAgSb $\gamma 1$-phase (see Table 1) using the phono3py program and the WIEN2k interface developed by us for the phono3py program. Next, the WIEN2k program was used to calculate the electronic structure of a set of supercells in order to find the forces acting on the atoms resulting from the displacement of individual atoms in the supercells. The PBE functional was used in the calculations as an exchange-correlation functional [38], which makes it possible to optimize the lattice parameters and coordinates of atoms in the lattice cell and is a variant of the generalized gradient approximation (GGA). The calculations were performed without taking into account the spin-orbit interaction. The parameters set to achieve the required accuracy in the calculations were the same as those used in the calculations of the electronic band structure of α-, β-, $\gamma 1$- and $\gamma 2$-phases of the MgAgSb compound. After processing the results of calculations of the electronic structure of a set of supercells, the phono3py program generated files with force constants of the 2nd and 3rd orders, on the basis of which phonopy program was used to calculate phonon spectra. At the final stage, the linearized kinetic Boltzmann equation for phonons was solved iteratively using the phono3py program and the lattice thermal conductivity was calculated. The obtained vibrational spectra and the lattice thermal conductivity of the MgAgSb $\gamma 1$-phase are shown in Figure 3, *a, b*.

The results of the calculations of the phonon spectra shown in Figure 3, *a* turned out to be close to the theoretical phonon spectra of the MgAgSb $\gamma 1$-phase obtained in Ref. [7]. A solid line in Figure 3, *b* indicates the calculated values of lattice thermal conductivity for the temperature range of 600–800 K, in which MgAgSb $\gamma 1$-phase either co-exists with the β-phase (from 600 to 700 K) according to experimental data [6,7], or is present as the only stable

phase (from 700 to 800 K). The dotted line shows the values of thermal conductivity in the temperature ranges 800–1000 and 300–600 K. The coexistence of $\gamma 1$- and $\gamma 2$-phases of MgAgSb was recorded in the first high-temperature region [7] and the presence of $\gamma 1$-phase was found in the second region when the sample was cooled [6]. We are aware of only one study in Ref. [7], which provides experimental data for the thermal conductivity κ_{tot} of MgAgSb in a wide temperature range from 300 to 710 K, partially covering the area of existence of MgAgSb $\gamma 1$-phase. The calculated numerical values of κ_{lat} in Figure 3, *b* in the temperature range of 600–700 K do not contradict the experimental data [7].

4. Calculations of mechanical properties of MgAgSb crystal phases

The mechanical properties of tetragonal α-, β- and cubic $\gamma 1$-, $\gamma 2$-phases of the MgAgSb compound were modeled using the IRelast program [34], implemented in the WIEN2k suite of programs [19]. The PBE [38] functional recommended in Ref. [34] was used as an exchange-correlation functional. It is assumed that Hooke's law holds for the material [39]:

$$\sigma_{ij} = c_{ijkl}\varepsilon_{kl}, \tag{3}$$

where σ_{ij} is the stress tensor, ε_{kl} is the strain tensor, c_{ijkl} is the elastic modulus tensor (tensor of elastic stiffness constants). Each of the indexes i, j, k, l can take values of Cartesian coordinates x, y, z. Due to the symmetry of the tensor of elastic moduli in pairs of subscripts $c_{ijkl} = c_{jilk}$, the relation (3) is usually written in Voigt notation [39]:

$$\sigma_i = c_{ij}\varepsilon_j, \tag{4}$$

where $i, j = 1, 2, 3, 4, 5, 6$ and the digits $1, 2, \ldots 6$ correspond to pairs of Cartesian coordinates: xx; yy; zz; yz, zy; xz, zx; xy, yx. Due to the symmetry properties [39], the number of independent elastic moduli for cubic crystals is equal to three: c_{11}, c_{12}, c_{44}, and six for tetragonal crystals: $c_{11}, c_{12}, c_{13}, c_{33}, c_{44}, c_{66}$. The criteria for the mechanical stability of lattices impose the following conditions on elastic moduli for cubic crystals (Born criteria [40]):

$$c_{11} > c_{12}, \quad c_{44} > 0, \quad c_{11} + 2c_{12} > 0. \tag{5}$$

The following criteria were proposed for mechanical stability for tetragonal crystals in a number of articles [41,42]:

$$c_{11} > 0, \quad c_{33} > 0, \quad c_{44} > 0, \quad c_{66} > 0, \quad c_{11} - c_{12} > 0,$$

$$c_{11} + c_{33} - 2c_{13} > 0, \quad 2c_{11} + 2c_{12} + c_{33} + 4c_{13} > 0. \tag{6}$$

However, the criteria (6) for tetragonal crystals are called erroneous in Ref. [43]. The following conditions are proposed in Ref. [43] instead of (6):

$$c_{11} > |c_{12}|, \quad c_{44} > 0, \quad c_{66} > 0,$$

$$(c_{11} + c_{12})c_{33} > 2c_{13}^2. \tag{7}$$

The crystal energy is decomposed into a series of small deformations up to the 2nd order terms in the IRelast [34] program, assuming that Hooke's law is fulfilled:

$$E(V, \varepsilon_k) = E_0 + V_0\left(\sum_{i=1}^{6}\sigma_i\varepsilon_i + \frac{1}{2}\sum_{i,j=1}^{6}c_{ij}\varepsilon_i\varepsilon_j\right), \tag{8}$$

where E_0 and V_0 are the energy and volume of an undeformed crystal, and E and V are the energy and volume of a deformed crystal subjected to deformation $\varepsilon_1, \ldots, \varepsilon_6$ which are specifically selected for different crystal symmetries. The elastic constants are found using the second derivative of the strain energy under the condition $\varepsilon_k = 0$:

$$c_{ij} = \frac{1}{V_0}\left(\frac{\partial^2 E}{\partial\varepsilon_i\partial\varepsilon_j}\right)\Big|_{\varepsilon_k=0}. \tag{9}$$

In addition to elastic moduli c_{ij}, the IRelast [34] program also finds macroscopic strength characteristics of crystals such as shear modulus G, bulk modulus B, Young's modulus E, Poisson's ratio ν. Three approaches are used to calculate them, named after their authors: Voigt [44], Reuss [45] and Hill [46]. With the exception of the bulk moduli of cubic crystals, for which the equality $B_{\text{V}} = B_{\text{R}}$, is valid, for all other moduli the Voigt's approximation is considered an upper-bound estimate, the Reuss approximation is a lower-bound estimate, and the Hill moduli are calculated as the arithmetic mean of the Voigt and Reuss moduli. The shear modulus G is the crystal's response to reversible deformation caused by shear stress. The Voigt shear modulus G_{V} and Reuss shear modulus G_{R} for cubic crystals are expressed in terms of the following combinations of elastic moduli [42]:

$$G_{\text{V}} = \frac{1}{5}(c_{11} - c_{12} + 3c_{44});$$

$$G_{\text{R}} = \frac{5(c_{11} - c_{12})c_{44}}{4c_{44} + 3(c_{11} - c_{12})}. \tag{10}$$

The bulk modulus B demonstrates the crystal's response to uniform hydrostatic pressure. The following expression is used for cubic crystals [42]:

$$B_{\text{V}} = B_{\text{R}} = \frac{1}{3}(c_{11} + 2c_{12}). \tag{11}$$

The ratio B/G (Pugh's ratio [47]) is used for evaluation of the ductility or brittleness of a material. If $B/G > 1.75$, then the material is considered plastic.

For crystals with tetragonal symmetry, the bulk and shear moduli are expressed in terms of elastic moduli as follows [48]:

$$B_{\text{V}} = \frac{1}{9}[2(c_{11} + c_{12}) + c_{33} + 4c_{13}];$$

$$G_{\text{V}} = \frac{1}{30}(7c_{11} - 5c_{12} + 2c_{33} - 4c_{13} + 12c_{44}). \tag{12}$$

$$B_{\mathrm{R}} = \frac{(c_{11}+c_{12})c_{33}-2c_{13}^2}{c_{11}+c_{12}+2c_{33}-4c_{13}};$$

$$G_{\mathrm{R}} = 15\left[\frac{18B_{\mathrm{V}}}{(c_{11}+c_{12})c_{33}-2c_{13}^2} + \frac{6}{(c_{11}-c_{12})} + \frac{6}{c_{44}} + \frac{3}{c_{66}}\right]^{-1}. \quad (13)$$

The Young's modulus E, which is a measure of the stiffness of a crystal, and the Poisson's ratio ν, which characterizes the shear stability of a crystal, are related to the bulk modulus B and the shear modulus G by known ratios [39]:

$$E = \frac{9BG}{3B+G}; \quad \nu = \frac{3B-2G}{6B+2G}. \quad (14)$$

Moreover, the IRelast program [34] calculates Vickers hardness using two empirical formulas — Chen's [49] and Tian's formulas [50]:

$$H_{\mathrm{V,Chen}} = 2(k^2G)^{0.585} - 3;$$

$$H_{\mathrm{V,Tian}} = 0.92k^{1.137}G^{0.708}, \quad (15)$$

where $k = G/B$ is the parameter inverse to the Pughs's ratio [47], as well as the Ranganathan's anisotropy index A^{U} [51] and the Kube's anisotropy index A^{L} [52]:

$$A^{\mathrm{U}} = \frac{B_{\mathrm{V}}}{B_{\mathrm{R}}} + \frac{5G_{\mathrm{V}}}{G_{\mathrm{R}}} - 6;$$

$$A^{\mathrm{L}} = \left\{\left[\ln\left(\frac{B_{\mathrm{V}}}{B_{\mathrm{R}}}\right)\right]^2 + 5\left[\ln\left(\frac{G_{\mathrm{V}}}{G_{\mathrm{R}}}\right)\right]^2\right\}^{1/2}. \quad (16)$$

Table 3 shows the results of calculations of the mechanical properties of α-, β-, $\gamma 1$- and $\gamma 2$-phases of the MgAgSb compound, performed using the IRelast program [34]. In particular, Table 3 shows the values of elastic moduli c_{ij}, shear moduli G, bulk moduli B, Young's moduli E and Poisson's ratio ν in Voigt's, Reuss' and Hill's formulations (10)–(14), Pugh's ratios B/G, Vickers hardness $H_{\mathrm{V,Chen}}$ and $H_{\mathrm{V,Tian}}$ (15), and Ranganathan's anisotropy index A^{U} and Kube's anisotropy index A^{L} (16). The values of all moduli and hardness values are given in GPa. All other characteristics (ν, B/G, A^{U} and A^{L}) are dimensionless.

From the calculation results presented in Table 3, a number of conclusions can be drawn about the mechanical strength properties of MgAgSb.

1. The numerical values of the elastic constants c_{ij} satisfy the mechanical stability conditions (5)–(7) for all phases of MgAgSb.

2. All MgAgSb phases should have plastic properties, since the Pugh's ratio [47] $B_{\mathrm{H}}/G_{\mathrm{H}}$ for them exceeds 1.75.

3. The values of the Poisson's ratio for all MgAgSb phases are higher than typical values: 0.10 for covalent [53] and 0.25 for ionic crystals [54,55]. This fact is in agreement with the type of chemical bonding in all MgAgSb phases, revealed by the analysis of BCPs parameters given in Table 2.

Table 3. Mechanical properties of α-, β-, $\gamma 1$- and $\gamma 2$-phases of the MgAgSb compound

Properties	α-phase	β-phase	$\gamma 1$-phase	$\gamma 2$-phase
c_{11}	111.77	100.39	74.43	66.89
c_{12}	39.85	29.86	57.24	43.67
c_{13}	53.75	50.81	57.24	43.67
c_{33}	103.48	91.68	74.43	66.89
c_{44}	39.88	28.09	48.99	40.92
c_{66}	27.35	5.11	48.99	40.92
B_{V}	69.08	61.71	62.97	51.41
B_{R}	69.03	61.41	62.97	51.41
B_{H}	69.05	61.56	62.97	51.41
G_{V}	33.40	22.99	32.83	29.20
G_{R}	31.98	14.29	17.01	20.36
G_{H}	32.69	18.64	24.92	24.78
B/G	2.11	3.30	2.53	2.08
E_{V}	86.30	61.35	83.91	73.65
E_{R}	83.12	39.79	46.82	53.96
E_{H}	84.71	50.80	66.05	64.05
ν_{V}	0.292	0.334	0.278	0.261
ν_{R}	0.299	0.392	0.376	0.325
ν_{H}	0.296	0.362	0.325	0.292
$H_{\mathrm{V,Chen}}$	3.41	−0.26	1.44	2.57
$H_{\mathrm{V,Tian}}$	4.64	1.88	3.13	3.89
A^{U}	0.22	3.05	4.65	2.17
A^{L}	0.010	1.06	1.47	0.81

4. MgAgSb β-phase has the worst Vickers hardness values $H_{\mathrm{V,Chen}}$ and $H_{\mathrm{V,Tian}}$ (15) compared to other phases, which can lead to deterioration of the mechanical properties of the sample in case of occurrence of a β-phase in it.

5. High values of the Ranganathan's anisotropy index A^{U} and Kube's anisotropy index A^{L} (16) for β-, $\gamma 1$- and $\gamma 2$-phases of MgAgSb can lead to formation of microcracks under mechanical loads [56].

6. MgAgSb α-phase has the best strength properties relative to other MgAgSb phases.

Comparison of the results of calculations of the mechanical properties of MgAgSb presented in Table 3 with experimental data is difficult due to their almost complete absence in the literature for β- and γ-phases. There are only a few articles that provide experimental data on the mechanical properties of stoichiometric samples of MgAgSb α-phase [27,57]. The most detailed studies of nanostructured samples of α-MgAgSb were performed in Ref. [57]. Processing the results of microhardness measurements using the technique proposed in Ref. [58] allowed the authors of the article [57] to obtain the value of the Young's modulus $E = 55$ GPa, less than E_{H} for α-MgAgSb from Table 3. While the nanohardness of 3.3 GPa found in Ref. [57] is close to the data for $H_{\mathrm{V,Chen}}$ and slightly less than $H_{\mathrm{V,Tian}}$ from Table 3. Experimental values of the longitudinal v_l and transverse v_t sound velocities for α-MgAgSb are given in Ref. [27] and are equal, respectively, to 3360 and 1715 m/s.

Using these data and the formula

$$B = \frac{\rho(3v_l^2 - 4v_t^2)}{3}, \quad (17)$$

where ρ is density, the value of the bulk modulus $B = 43.5$ HPa is found which is less than the value B_H for α-MgAgSb from Table 3. It should be noted that the values of $v_l = 4225$ m/s and $v_t = 2276$ m/s obtained for α-MgAgSb in this study using the IRelast program also turned out to be slightly higher than the corresponding sound velocity values given in Ref. [27]. The elastic moduli c_{ij}, bulk moduli B, shear moduli G, Young's modulus E and Poisson's ratio ν were calculated for MgAgSb α-, β- and γ1-phases in two theoretical papers [42,59] using the VASP computer software package [60] and the exchange-correlation functional PBE [38]. It should be noted that the values of the elastic modulus c_{44} given in Table 3 are noticeably higher than the values of c_{44} from Refs. [42,59]. The values of the moduli B, G and E from Table 3 turned out to be slightly higher than the corresponding values of the moduli given in Refs. [42,59]. The values of the Poisson's ratio ν in Table 3 and in Refs. [42,59] differ insignificantly.

5. Conclusion

Let us note the most significant results of this study.

1. Structural phase transitions between α-, β- and γ-phases of MgAgSb are accompanied by changes in the nature of the electronic band structure from semiconductor to metallic. As a result, the nature of the temperature dependences of the kinetic coefficients of conductivity σ, thermo-emf (Seebeck coefficient) S and thermal conductivity k should change significantly in case of phase transitions, which is observed in experiments [7].

2. The numerical parameters of the bond-type saddle critical points in the charge density distribution for all MgAgSb phases revealed the absence of a covalent chemical bonding in this compound, and also allowed us to establish that the type of chemical bonding in MgAgSb is similar to that found in phase change materials, as well as in high-temperature superconductors and parent compounds for obtaining them. This fact may explain the presence of several structural phase transitions in MgAgSb over a small temperature range, as well as low values of lattice thermal conductivity. The absence of a covalent bonding in MgAgSb is confirmed by the numerical values of the strength parameters of this compound.

3. An analysis of the calculated values of the strength mechanical properties of various phases of the MgAgSb compound showed that the α-phase has the best characteristics, which confirms the prospects of its use as a thermoelectric material in the temperature range of 300–600 K.

Funding

This study was carried out under the state assignment of the National Research Center „Kurchatov Institute“.

Conflict of interest

The authors declare that they have no conflict of interest.

References

[1] X. Zhang, H. Zhu, X. Dong, Z. Fan, Y. Yao, N. Chen, J. Yang, K. Guo, J. Hao, L. He, G. Li, H. Zhao. Joule, **8**, 3324 (2024).
[2] A. Wieder, J. Camut, A. Duparchy, R. Deshpande, A. Cowley, E. Müller, J. deBoor. Materials Today Energy, **38**, 101420 (2023).
[3] Z. Liu, N. Sato, W. Gao, K. Yubuta, N. Kawamoto, M. Mitome, K. Kurashima, Y. Owada, K. Nagase, C.-H. Lee, J. Yi, K. Tsuchiya, T. Mori. Joule, **5**, 1196 (2021).
[4] P. Ying, X. Liu, C. Fu, X. Yue, H. Xie, X. Zhao, W. Zhang, T.-J. Zhu. Chem. Mater., **27**, 909 (2015).
[5] H. Zhao, J. Sui, Z. Tang, Y. Lan, Q. Jie, D. Kraemer, K. McEnany, G. Chen, Z. Ren. Nano Energy, **7**, 97 (2014).
[6] M.J. Kirkham, A.M. dos Santos, C.J. Rawn, E. Lara-Curzio, J.W. Sharp, A.J. Thompson. Phys. Rev. B, **85**, 144120 (2012).
[7] J.-L. Mi, P.-J. Ying, M. Sist, H. Reardon, P. Zhang, T.-J. Zhu, X.-B. Zhao, B.B. Iversen. Chem. Mater., **29**, 6378 (2017).
[8] N. Miao, P. Ghoser. J. Phys. Chem. C, **119**, 1407 (2015).
[9] X. Tan, L. Wang, H. Shao, S. Yue, J. Xie, G. Liu, H. Jiang, J. Jiang. Adv. Energy Mater., **7**, 1700076 (2017).
[10] C.Y. Sheng, H.J. Liu, D.D. Fan, L. Cheng, J. Zhang, J. Wei, J.H. Liang, P.H. Jiang, J. Shi. J. Appl. Phys., **119**, 195101 (2016).
[11] Z. Feng, J. Zhang, Y. Yan, G. Zhang, C. Wang, C. Peng, F. Ren, Y. Wang, Z. Cheng. Sci. Rep., **7**, 2572 (2017).
[12] V.G. Orlov, G.S. Sergeev. Solid St. Commun., **258**, 7 (2017).
[13] V.G. Orlov, G.S. Sergeev. Kristallografiya **64**, 396 (2019). (in Russian).
[14] V.G. Orlov, G.S. Sergeev. FTT **59**, 1278 (2017). (in Russian).
[15] V.G. Orlov, G.S. Sergeev, E.A. Kravchenko. JMMM, **475**, 627 (2019).
[16] V.G. Orlov, G.S. Sergeev. Physica B, **536**, 839 (2018).
[17] V.G. Orlov, G.S. Sergeev. ZhETF **104**, 107 (2023). (in Russian).
[18] V.G. Orlov, G.S. Sergeev. J. Supercond. Novel. Magn., **38**, 61 (2025).
[19] P. Blaha, K. Schwarz, G.K.H. Madsen, D. Kvasnicka, J. Luitz, R. Laskowski, F. Tran, L.D. Marks. WIEN2k, An Augmented Plane Wave + Local Orbitals Program for Calculating Crystal Properties, revised edition WIEN2k_23_2 (Release 07/24/2024) (Karlheinz Schwarz, Vienna University of Technology, Austria, 2024). ISBN 3-9501031-1-2.
[20] P. Blaha, K. Schwarz, F. Tran, R. Laskowski, G.K.H. Madsen, L.D. Marks. J. Chem. Phys., **152**, 074101 (2020).
[21] F. Tran, P. Blaha. Phys. Rev. Lett., **102**, 226401 (2009).
[22] J.P. Perdew, Y. Wang. Phys. Rev. B, **23**, 13244 (1992).
[23] A. Otero-de-la-Roza, E.R. Johnson, V. Luaña. Comp. Phys. Commun., **185**, 1007 (2014).
[24] R.F.W. Bader. *Atoms in Molecules: A Quantum Theory. International Series of Monographs on Chemistry 22* (Oxford Science Publications, Oxford, 1990).

[25] C. Gatti. Z. Kristallogr., **220**, 399 (2005).
[26] *The Quantum Theory of Atoms in Molecules. From Solid State to DNA and Drug Design*, ed. by C.F. Matta, R.J. Boyd (WILEY-VCH Verlag GmbH&Co. KGaA, Weinheim, 2007).
[27] P. Ying, X. Li, Y. Wang, J. Yang, C. Fu, W. Zhang, X. Zhao, T. Zhu. Adv. Funct. Mater., **27**, 1604145 (2017).
[28] K.S. Lukas, W.S. Liu, G. Joshi, M. Zebarjadi, M.S. Dresselhaus, Z.F. Ren, G. Chen, C.P. Opeil. Phys. Rev. B, **85**, 205410 (2012).
[29] J. Yang, Y. Wang, H. Yang, W. Tang, J. Yang, L. Chen, W. Zhang. J. Phys.: Condens. Matter, **31**, 183002 (2019).
[30] J.-Y. Yang, W. Zhang, M. Hu. J. Appl. Phys., **125**, 205105 (2019).
[31] X. Li, P.-F. Liu, E. Zhao, Zh. Zhang, T. Guidi, M. Duc Le, M. Avdeev, K. Ikeda, T. Otomo, M. Kofu, K. Nakajima, J. Chen, L. He, Y. Ren, X.- L. Wang, B.-T. Wang, Zh. Ren, H. Zhao, F. Wang. Nature Commun., **11**, 942 (2020).
[32] A. Togo, I. Tanaka. Scripta Materialia, **108**, 1 (2015).
[33] A. Togo, L. Chaput, T. Tadano, I. Tanaka. J. Phys.: Condens. Matter, **35**, 353001 (2023).
[34] M. Jamal, M. Bilal, I. Ahmad, S. Jaladi-Asadabadi. J. Alloys Compd., **735**, 569 (2018).
[35] *Int. Tables for Crystallography*, v. A. *Space-group symmetry* (5th ed. Ed. by Th. Hahn (Springer, 2005).
[36] R. Arpaia, S. Caprara, R. Fumagalli, G.De. Vecchi, Y.Y. Peng, E. Andersson, D. Betto, G.M. Deluca, N.B. Brookes, F. Lombardi, M. Salluzzo, L. Braicovich, C.Di Castro, M. Grilli, G. Ghiringhelli. Science, **365**, 906 (2019).
[37] R. Arpaia, G. Chiringhelli. J. Phys. Soc. Jpn., **90**, 111005 (2021).
[38] J.P. Perdew, K. Burke, M. Ernzerhof. Phys. Rev. Lett., **77**, 3865 (1996).
[39] J.F. Nye. *Physical properties of Crystals* (Oxford University Press, London, 1959).
[40] M. Born. Math. Proc. Cambridge Philos. Soc., **36**, 160 (1940).
[41] Z. Wu, E. Zhao, H. Xiang, X.-F. Hao, X.-J. Liu, J. Meng. Phys. Rev. B, **76**, 054115 (2007).
[42] J. Wang, X. Fu, X. Zhang, J.-T. Wang, X.-D. Li, Z.-Y. Jiang. Chin. Phys. B, **25**, 086302 (2016).
[43] A.I. Gusev, S.I. Sadovnikov. FTT **64**, 671 (2022). (in Russian).
[44] W. Voigt. *Lehrbuch der Kristallphysik* (Leipzig, Teubner, 1928).
[45] A. Reuss. Z. Angew. Math. Mech., **9**, 94 (1929).
[46] R. Hill. Proc. Phys. Soc. London A, **65**, 349 (1952).
[47] S.F. Pugh. Philos. Mag., **45**, 823 (1954).
[48] J.P. Watt, L. Peselnick. J. Appl. Phys., **51**, 1520 (1980).
[49] X.-Q. Chen, H. Niu, D. Li, Y. Li. Intermetallics, **19**, 1275 (2011).
[50] Y. Tian, B. Xu, Z. Zhao. Int. J. Refr. Metals and Hard Mater., **33**, 93 (2012).
[51] S.I. Ranganathan, M. Ostoja-Starzewski. Phys. Rev. Lett., **101**, 055504 (2008).
[52] C.M. Kube. AIP Advances, **6**, 095209 (2016).
[53] J. Haines, J.M. Léger, G. Bocquillon. Ann. Rev. Mater. Res., **31**, 1 (2001).
[54] J.W. Soh, H.M. Lee, H.-S. Kwon. J. Alloys Compd., **194**, 119 (1993).
[55] A. Tasnim, Md. Mahamudujjaman, Md.A. Afzal, R.S. Islam, S.H. Naquib. Results Phys., **45**, 106236 (2023).
[56] V. Tvergraad, J.W. Hutchinson. J. Am. Ceram. Soc., **71**, 157 (1988).
[57] Z. Liu, W. Gao, X. Meng, X. Li, J. Mao, Y. Wang, J. Shuai, W. Cai, Z. Ren, J. Sui. Scr. Mater., **127**, 72 (2017).
[58] W.C. Oliver, G.M. Pharr. J. Mater. Res., **7**, 1564 (1992).
[59] G. Li, Q. An, U. Aydemir, S.I. Morozov, B. Duan, P. Zhai, Q. Zhang, W.A. Goggard III. J. Materiomics, **6**, 24 (2020).
[60] https://www.vasp.at.

Translated by A.Akhtyamov